Chinese Chemical Letters 33 (2022) 3859–3864

Contents lists available at ScienceDirect

Chinese Chemical Letters

journal homepage: www.elsevier.com/locate/cclet

Hierarchical metal-phenolic-polyplex assembly toward superwetting membrane for high-flux and antifouling oil-water separation

Xueting Zhao, Yuanyuan Jiang, Lijuan Cheng, Youyou Lan, Tingyuan Wang, Jiefeng Pan*, Lifen Liu*

College of Chemical Engineering, Zhejiang University of Technology, Hangzhou 310014, China

ARTICLE INFO

Article history:
Received 23 September 2021
Revised 31 October 2021
Accepted 8 December 2021
Available online 13 December 2021

Keywords:
Metal-phenolic
Polyplex
Superwetting
Membrane
Oil-water separation

ABSTRACT

Superwetting membranes have emerged as promising materials for the efficient treatment of oily wastewater. Typically, superwetting membranes can be developed by ingeniously chemical modification and topographical structuration of microporous membranes. Herein, we report the hierarchical assembly of metal-phenolic-polyplex coating to manipulate membrane surface superwettability by integrating metal-phenolic (Fe^{III}-tannic acid (TA)) assembly with polyplex (tannic acid-polyethylenimine (PEI)) assembly. The proposed Fe-TA-PEI coating can be deposited on microporous membrane *via* simply dipping into Fe^{III}-TA-PEI co-assembly solution. Based on the catechol chemistry, the coordination complexation of Fe^{III} and TA develops metal-phenolic networks to provide hydrophilic chemistries, and the electrostatic complexation of TA and PEI generates nanoconjugates to impart hierarchical architectures. Benefiting from the synergy of hydrophilic chemistries and hierarchical architectures, the resulting PVDF/Fe-TA-PEI membrane exhibits excellent superhydrophilicity (~0°), underwater superoleophobicity (~150°) and superior anti-oil-adhesion capability. The superhydrophilicity of PVDF/Fe-TA-PEI membrane greatly promotes membrane permeability, featuring water fluxes up to 5860 L m^{-2} h^{-1}. The underwater superoleophobicity of PVDF/Fe-TA-PEI membrane promises potential flux (3393 L m^{-2} h^{-1}), high separation efficiency (99.3%) and desirable antifouling capability for oil-in-water emulsion separation. Thus, we highlight the reported hierarchical metal-phenolic-polyplex assembly as a straightforward and effective strategy that enables the synchronous modulation of surface chemistry and topography toward superwetting membranes for promising high-flux and antifouling oil-water separation.

With the development of petrochemical industry, the ever-growing amount of oily wastewater is generated during the exploration, transportation, storage and processing of petroleum or related products, which threatens aquatic ecosystems and endangers human life [1–3]. Advanced technologies for efficient oily wastewater treatment are highly desired. Membrane technologies have been regarded as the promising candidates with the advantages of high efficiency, low energy consumption, ease of process, scalability and integration [4,5]. Oil-water separation membranes are the cores of membrane technologies for oily wastewater treatment. However, most commercial membranes (such as microfiltration and ultrafiltration membranes) suffer from the high tendency towards membrane fouling, which sacrifice permeability, separation efficiency and membrane life [6–8]. Therefore, the exploration of advanced high-performance oil-water separation membranes is the major premise of promoting the practical application of membrane technologies in oily wastewater treatment.

In recent years, superwetting materials provide a new perspective for the development of high-performance oil-water separation membrane [9–14]. Based on superwetting theory, a superhydrophilic surface can trap dense hydration layer at the water-solid interface and further present underwater superoleophobicity by employing the hydration layer to repel oil foulants [15–17]. It can be expected that superhydrophilic and underwater superoleophobic membranes will be helpful to overcome the disadvantages of membrane fouling. Since Jiang and co-workers first reported on the mechanism of low-adhesive superoleophobic phenomena in water in 2009 [18] and further applied the mechanism to direct the design of oil-water separation membrane [19,20], the development of superhydrophilic and underwater superoleophobic oil-water separation membranes has become the focus of recent researches. Various membranes with superhydrophilicity and underwater

* Corresponding authors.
E-mail addresses: panjiefeng@zjut.edu.cn (J. Pan), lifenliu@zjut.edu.cn (L. Liu).

https://doi.org/10.1016/j.cclet.2021.12.017
1001-8417/

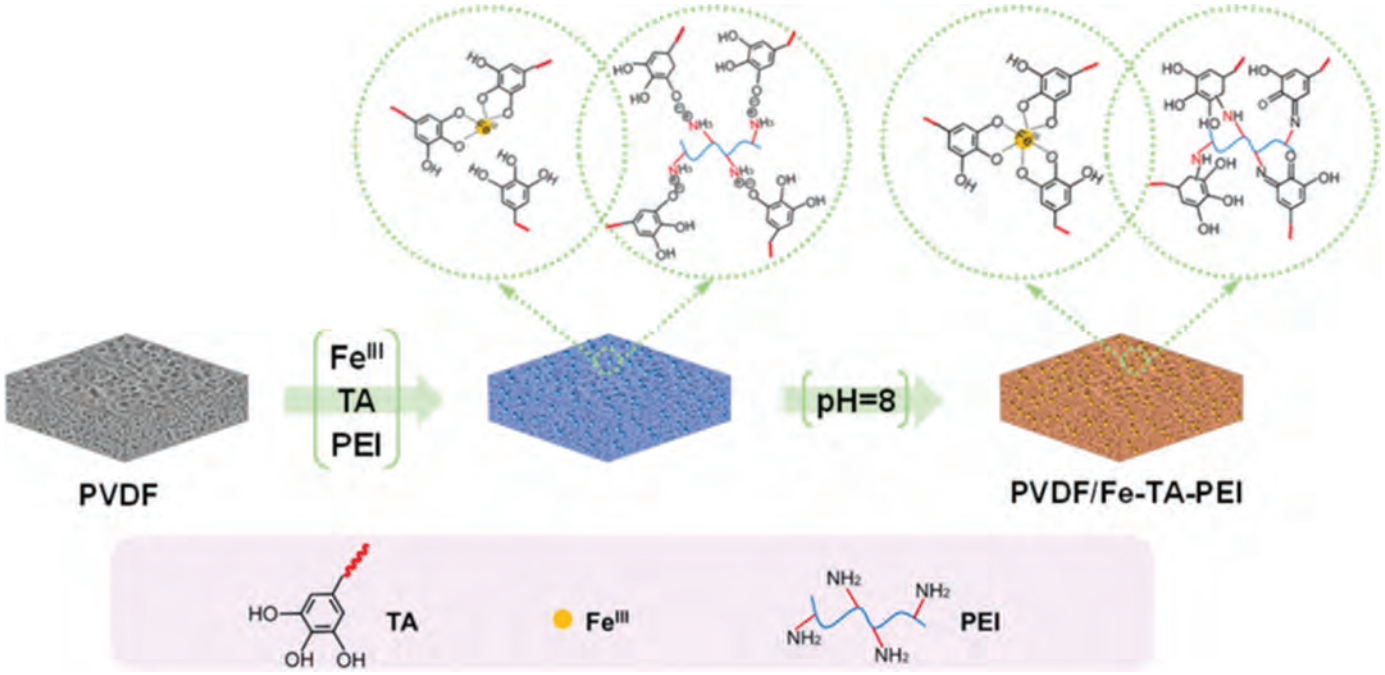

Fig. 1. Schematic illustration for the hierarchical assembly process of metal-phenolic-polyplex coating on membrane surface.

superoleophobicity for effective oil-water separation have been fabricated *via* surface coating [21–25], surface grafting [26–28], templating [29], nanomaterial depositing/growing [30–33], and so on. The micro/nanohierarchically structured and highly hydrated surface characteristics have great impacts on membrane superwettability. Both inorganic and organic nanomaterials are employed to construct unique micro/nanohierarchical architectures [30–37], and both polyelectrolytes and bioinspired minerals are employed to impart hydrophilic moieties [38–41]. Despite remarkable progress, the facile route to directly construct hydrophilic hierarchical architectures on membrane surface is still highly demanded.

Metal-phenolic networks (MPNs) have become an emerging class of coatings derived from the coordination assembly of multivalence metal ions and multidentate phenolic ligands since first reported by Caruso and co-workers in 2013 [42]. Thanks to the strong affinity of polyphenols towards various substrates and the strong intermolecular cross-linking by metal ions, MPN assembly can provide a facile and efficient way for material engineering and surface functionalization [43,44]. MPNs modified membranes have recently attracted considerable interest due to their inherent hydrophilicity, multiple interactions and reliable adhesion capability. As reported recently, hydrophilic MPN coatings are favorable for tailoring the superhydrophilicity and underwater superoleophobicity of membrane surface [45–49]. Although usual one-step assembly and discrete assembly routes have been developed to create MPN coatings, the majority of them fail to simultaneously construct critical micro/nanohierarchical rough structures. For engineering reliable superhydrophilic and underwater superoleophobic oil-water separation membranes, the straightforward route to tailor ingenious MPN coatings into hydrophilic hierarchical architectures is still desired.

In our previous study, we have demonstrated the potential of MPN coating derived from polyphenol-polycation-metal complexation for fabrication superwetting membranes [50]. However, the assembly route still remains some problems such as tedious steps and the discrete control of nanoconjugate generation. Aiming to synthesis of MPN-based superwetting membranes through a facile and straightforward route, we developed a one-step co-assembly

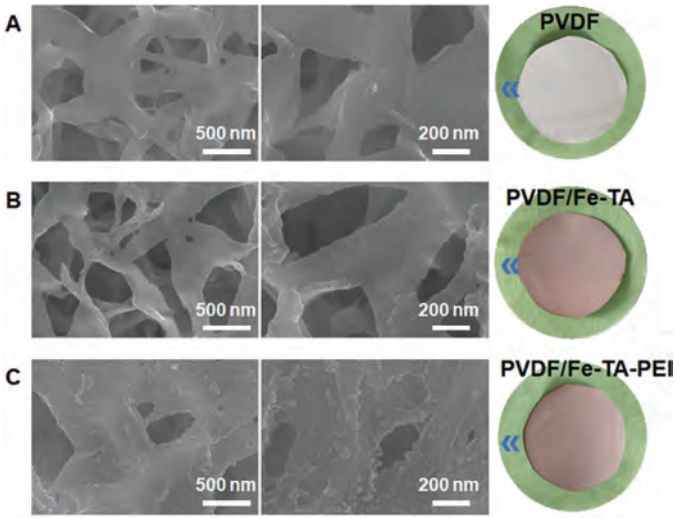

Fig. 2. The SEM and photo images of (A) the original PVDF, (B) PVDF/Fe-TA and (C) PVDF/Fe-TA-PEI membranes.

route to control the continuous growth of MPN coating. Herein, the hierarchical assembly of metal-phenolic-polyplex coating was proposed for the first time and completed in single coating step by dipping into pre-complex solutions of phenolic ligands (tannic acid, TA), metal ions (Fe^{III}) and polycation (polyethylenimine, PEI) (Fig. 1). The critical point of this route lied in integrating metal-phenolic (Fe^{III}-TA) assembly with polyplex (TA-PEI) assembly, where the coordination complexation of Fe^{III} and TA deposited hydrophilic MPNs onto membrane surface, and the electrostatic complexation of TA and PEI decorated hierarchical nanoconjugates with MPNs. The as-prepared PVDF/Fe-TA-PEI membrane was successfully structured with hydrophilic hierarchical architectures and showed greatly promoted membrane superwettability, permeation and emulsion separation performance and antifouling capability.

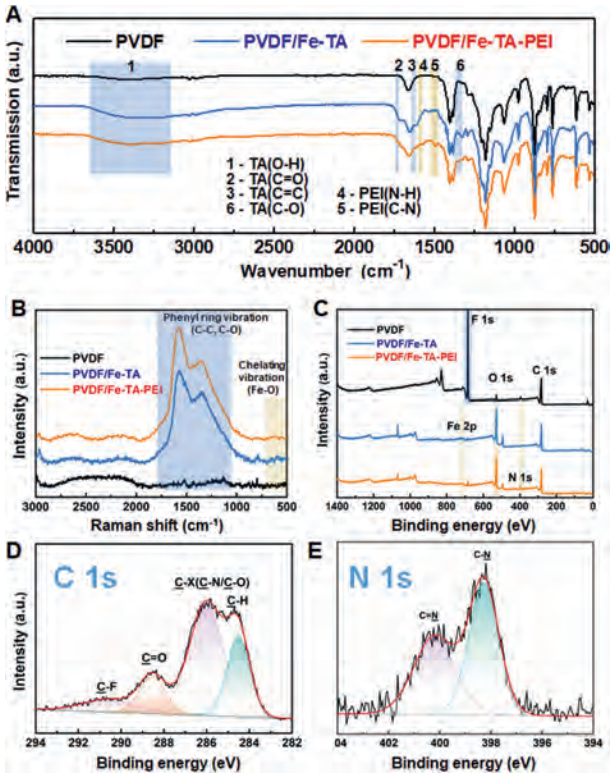

Fig. 3. (A) FTIR, (B) Raman, (C) XPS survey spectra of the original PVDF, PVDF/Fe-TA and PVDF/Fe-TA-PEI membranes. (D, E) XPS curve fitting of C 1s and N 1s spectra of the PVDF/Fe-TA-PEI membrane.

To confirm the formation of hierarchical rough Fe-TA-PEI coating, scanning electron microscopy (SEM) was first applied to the characterization of the surface morphology of different membranes (Fig. 2). The original PVDF membrane showed a clear and smooth surface morphology (Fig. 2A). After deposition of Fe-TA coating, the PVDF/Fe-TA membrane was evenly covered with Fe-TA aggregates, while still having a relatively smooth surface morphology (Fig. 2B). As for the PVDF/Fe-TA-PEI membrane, the surface morphology became rougher with the addition of PEI into the Fe-TA assembly system. Evenly distributed nano-scale protuberances could be observed on membrane surface (Fig. 2C). The hierarchically rough surface morphology of the PVDF/Fe-TA-PEI membrane could be attributed to the formation of TA-PEI polyplex nanoconjugates *via* electrostatic interaction [51,52].

To further confirm the chemical compositions of different membranes, the Fourier transform infrared spectroscopy (FTIR), Raman and X-ray photoelectron spectroscopy (XPS) results are displayed in Fig. 3. As shown in the FTIR spectra (Fig. 3A), compared with the original PVDF membrane, the FTIR spectra of the PVDF/Fe-TA membrane presented a characteristic peak corresponding to the stretching vibration of phenolic −OH groups at 3200∼3600 cm^{-1}. The new peaks at 1708 cm^{-1}, 1608 cm^{-1} and 1325 cm^{-1} were ascribed to the C=O, C=C and C−O stretching vibration from TA molecule, respectively. These results confirmed the deposition of Fe-TA coating on the PVDF membrane surface. For the PVDF/Fe-TA-PEI membrane, the adsorption peaks at 1573 cm^{-1} and 1490 cm^{-1} appeared corresponding to the N−H bending and C−N stretching vibration in PEI molecule. The phenolic O−H and C−O stretching vibration peaks became weakened, revealing that the catechol groups partially coupled with PEI through electrostatic interaction or Schiff base reaction [51]. Raman studies were utilized to further reveal the formation of Fe-TA coordination (Fig. 3B and Fig. S2 in Supporting information). The Raman spectra confirmed the presence of substituted phenyl ring vibration peaks (C−C, C−O) in the high-frequency region from ∼1000 cm^{-1} to ∼2000 cm^{-1} [53] and the presence of Fe−O vibration due to catechol-Fe^{III} chelating in the low-frequency region from ∼500 cm^{-1} to ∼650 cm^{-1} [54] in the PVDF/Fe-TA and PVDF/Fe-TA-PEI membranes. The results of FTIR and Raman confirmed that the Fe-TA-PEI coating was successfully assembled on membrane surface.

Moreover, XPS studies were utilized to analyze the detailed evaluation of chemical compositions, and the results are shown in Figs. 3C-E and Fig. S1 (Supporting information). From XPS survey spectra (Fig. 3C), the peak of F element (at 710.4 eV) from PVDF membrane substrate was almost disappeared for the PVDF/Fe-TA and PVDF/Fe-TA-PEI membranes, and the intensity of O element (at 532 eV) was greatly enhanced, confirming the formation of Fe-TA and Fe-TA-PEI coating, respectively. For the PVDF/Fe-TA-PEI membrane, the peak of Fe 2p (Fig. S2) should be due to Fe-TA coordination, and the peak of N 1s (Fig. 3E) should be due to the incorporation of PEI. From the detailed XPS curve fitting of C 1s spectra, the PVDF/Fe-TA-PEI membrane (Fig. 3D) presented four curve-fitted peaks at 284.5 eV, 285.8 eV, 288.4 eV and 290.6 eV, which belonged to C−H, C−X (C−N or C−O), C=O and C−F, respectively. The N 1s core level spectra (Fig. 3E) could be curve-fitted into the peaks at binding energies of 398.4 eV and 400.3 eV corresponding C−N and C=N, respectively. The presence of C=N bond indicated that covalent bonding was formed between TA and PEI through Schiff base reaction.

The above results provided insights into the possible assembly mechanism of the Fe-TA-PEI coating (Fig. 4). When the membrane substrate was first immersed in the precomplexed Fe^{III}-TA-PEI solution, TA molecules with robust adhesion property were immobilized on the surface and complexed with Fe^{III} *via* coordination interaction in form of MPNs. Simultaneously, PEI molecules formed polyplex with TA *via* electrostatic interaction. Upon the ever growing of Fe-TA-PEI complexes, PEI manipulated the aggregate states of TA into nanoconjugates, and thus the Fe-TA-PEI complexes further fused and developed into hierarchical coating. The following immersion in weak alkali environment further facilitated the formation of covalent TA-PEI cross-linking *via* Michael addition and Schiff base reaction, and enhanced the coordination Fe^{III}-TA and Fe^{III}-PEI cross-linking *via* deprotonation of catechol groups and neutralization of amino groups. The multiple cross-linking interaction promised the stability of Fe-TA-PEI coating (Fig. S3 in Supporting information).

Given the successful assembly of hierarchical Fe-TA-PEI coating on membrane surface and their potential hydrophilicity, it was plausible that the PVDF/Fe-TA-PEI membrane could exhibit robust superhydrophilic and underwater superoleophobic properties. To investigate the wettability of the PVDF/Fe-TA-PEI membranes, both water contact angles (WCA) and underwater oil contact angles (UOCA) of different membranes were measured systematically, as shown in Figs. 5A and B.

Fig. 5A presents the evolution of WCAs of the PVDF, PVDF/Fe-TA and PVDF/Fe-TA-PEI membranes upon drop ages. For the PVDF membrane, the initial WCA was about 104.1° and slightly decreased to 97.7°, confirming the inherent hydrophobicity of the PVDF membrane. For the PVDF/Fe-TA and PVDF/Fe-TA-PEI membranes, the initial WCAs were both significantly decreased. The effect of hydrophilic MPNs contributed to the great hydrophilicity of both PVDF/Fe-TA and PVDF/Fe-TA-PEI membranes, and thus water droplets could quickly spread and infiltrate on membrane surfaces with the final WCAs of 0°. Notably, the PVDF/Fe-TA-PEI membrane exhibited the outstanding superhydrophilicity with the lowest initial WCA of 23.8° and the shortest wetting time within 1 s. The above observation indicated that both hydrophilic MPNs and hierarchical nanoconjugates played important roles in the water superwettability of membranes. Moreover, the Fe-TA-PEI

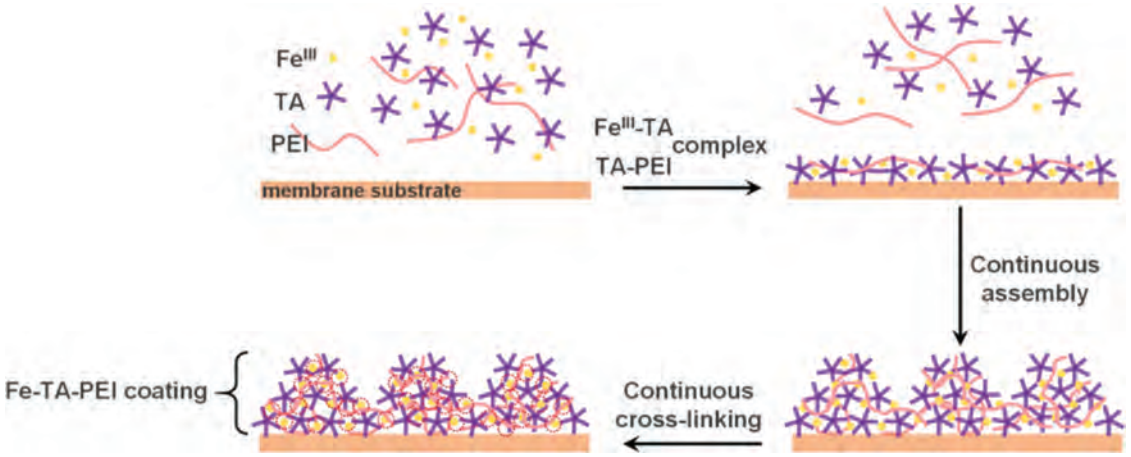

Fig. 4. Illustration of the assembly mechanism of the Fe-TA-PEI coating.

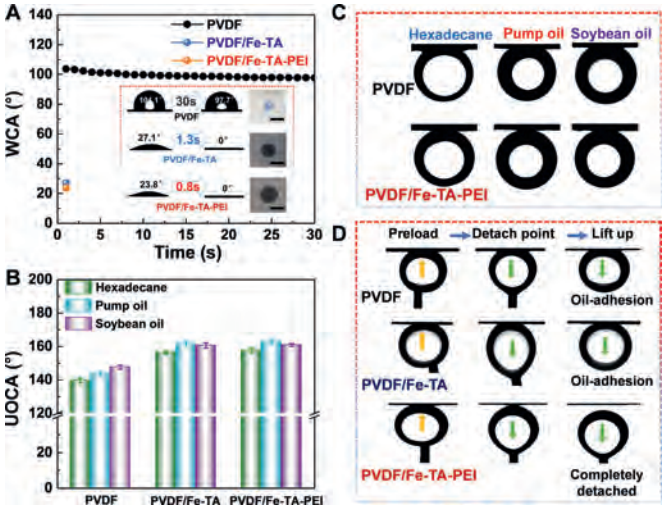

Fig. 5. (A) Water contact angles of the original PVDF, PVDF/Fe-TA and PVDF/Fe-TA-PEI membranes. Inset: Water wetting photographs (scale bar: 1 cm). (B) Underwater oil contact angles of different membranes subjected to different oil droplets. (C, D) Photographs of oil droplets and dynamic oil adhesion tests on the PVDF, PVDF/Fe-TA and PVDF/Fe-TA-PEI membranes in water.

coating could also be used to prepare superhydrophilic Nylon, MCE and PES membranes (Fig. S4 in Supporting information), further proving the universality of this strategy.

Generally, superhydrophilic surfaces can form a hydration layer that acts as a self-cleaning barrier against oils, and thus obtain underwater superoleophobic surfaces. To further evaluate the underwater oil repelling behavior of the membranes, three typical oils (hexadecane, pump oil and soybean oil) were applied to the PVDF, PVDF/Fe-TA and PVDF/Fe-TA-PEI membranes, as shown in Figs. 5B and C. The PVDF membrane showed an oleophobic feature with the UOCAs of all oil droplets lower than 145°. It could be clearly seen that the PVDF/Fe-TA and PVDF/Fe-TA-PEI membranes exhibited higher oil repelling behavior for various oils with all UOCAs above 155°, indicating underwater superoleophobicity. The underwater superoleophobicity of the PVDF/Fe-TA-PEI membrane could stand for a few days (Fig. S5 in Supporting information).

To better reveal the underwater superoleophobicity of the PVDF/Fe-TA-PEI membrane, the dynamic oil adhesion tests were carried out, and the result was shown in Fig. 5D. For the PVDF membrane, the preloaded oil could not be removed and finally adhered to membrane surface, indicating the higher oil adhesion tendency of the PVDF membrane. Despite underwater superoleophobicity of the PVDF/Fe-TA membrane, the preloaded oil still adhered to membrane surface, probably because the hydration layer was loose and easily replaced by preloaded oil. By comparison, the preloaded oil on the PVDF/Fe-TA-PEI membrane could completely detach from membrane surface without obvious residual or deformation, indicating the robust underwater superoleophobicity and anti-oil-adhesion property of the PVDF/Fe-TA-PEI membrane. The hydrophilic hierarchical architectures of the PVDF/Fe-TA-PEI membrane played critical roles to the underwater superoleophobic and anti-oil-adhesion characteristics. The hydrophilic groups of the Fe-TA-PEI coating adsorbed water molecules to form hydration layer, and the hierarchical structures of the Fe-TA-PEI coating confined the hydration layer within nanoconjugate patterns. The confined hydration layer decreased the contact area between oil and membrane surface and brought additional energy barrier for oil penetration, which prominently enhanced underwater superoleophobicity and oil repellency [31,55].

Since the Fe-TA-PEI coating was deposited throughout the membrane (Fig. S6 in Supporting information), the synchronous modification of both membrane surface and inner membrane pores was also promising to guarantee efficient water diffusion and permeation. Fig. 6A presents the permeation performance of the PVDF, PVDF/Fe-TA and PVDF/Fe-TA-PEI membranes. The PVDF/Fe-TA-PEI membrane exhibited the highest pure water flux of about 5860 L m^{-2} h^{-1}, being about 1.5 times that of the PVDF membrane (3458 L m^{-2} h^{-1}). The enhancement of water permeability was mainly related to the transformation of membrane wettability from hydrophobicity to superhydrophilicity. Superhydrophilic modification of membrane surface and pores could decrease water transport resistance and favor water permeation.

The desired superhydrophilicity, underwater superoleophobicity and anti-oil-adhesion property of the PVDF/Fe-TA-PEI membrane held great potential in high-flux and antifouling oil/water separation. The emulsion separation performance of different membranes was evaluated using pump oil-in-water emulsion (1 g/L). As shown in Fig. 6B, the hierarchical assembly of the superhydrophilic and underwater superoleophobic Fe-TA-PEI coating significantly enhanced the membrane permeation fluxes for emulsion separation from 847 L m^{-2} h^{-1} to 3393 L m^{-2} h^{-1}. There could be two reasons for this phenomenon. First, the high permeability of the PVDF/Fe-TA-PEI membrane promised the efficient transmembrane transport of water phase. Second, the underwater superoleophobicity and size exclusion of the PVDF/Fe-TA-PEI membrane inhibited both surface oil-spreading and inner oil-blocking, which retained more effective passages for water to pass through. Furthermore,

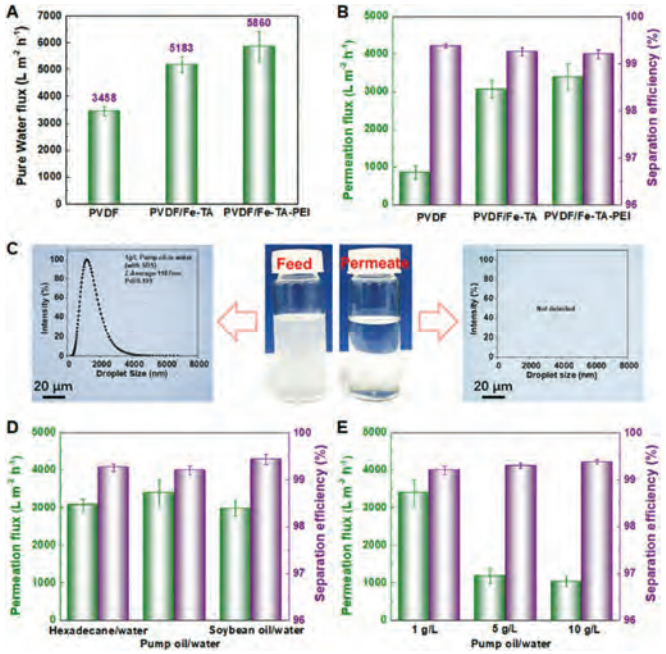

Fig. 6. (A) Pure water fluxes of the original PVDF, PVDF/Fe-TA and PVDF/Fe-TA-PEI membranes. (B) Permeation flux and corresponding separation efficiency of original PVDF, PVDF/Fe-TA and PVDF/Fe-TA-PEI membranes for the separation of pump oil-in-water emulsion. (C) Microscopy images and DLS data of pump oil-in-water emulsions before and after filtration using the PVDF/Fe-TA-PEI membrane. (D, E) Permeation fluxes and separation efficiency of the PVDF/Fe-TA-PEI membrane for the separation of different oil-in-water emulsions.

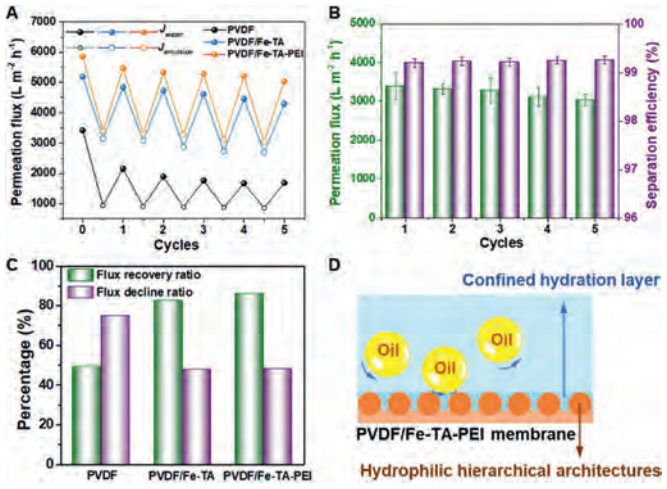

Fig. 7. (A) Cycling water and emulsion filtration test of the original PVDF, PVDF/Fe-TA, PVDF/Fe-TA-PEI membrane (using 1 g/L pump oil/water emulsion). (B) Permeation flux and separation efficiency of the PVDF/Fe-TA-PEI membrane for each cycle. (C) Summary of flux recovery ratio and total flux decline ratio after cycling tests. (D) Schematic illustration of the proposed antifouling mechanism of the PVDF/Fe-TA-PEI membrane.

all membranes showed high separation efficiency above 99.3%. The optical microscopy images and size distribution of pump oil-in-water emulsions were shown in Fig. 6C. After filtration, there was no detectable droplet in the clear filtrate, suggesting that the oil droplets were effectively removed.

Furthermore, we also tested the emulsion separation performance of the PVDF/Fe-TA-PEI membrane toward various oil-in-water emulsions. Fig. 6D shows the permeation fluxes and separation efficiency of the PVDF/Fe-TA-PEI membrane for the separation of hexadecane/water, soybean oil/water and pump oil/water emulsions, where it could be found that PVDF/Fe-TA-PEI membrane could maintain high permeation fluxes of more than 3000 L m^{-2} h^{-1} for various emulsions. Fig. 6E indicated that the permeation fluxes were related to the oil content in emulsions. Oil droplets at high oil content could lead to the loss of permeation flux because of their high accumulation tendency on membrane surface during filtration. Size distributions of the oil-in-water emulsions were given in Fig. S7 (Supporting information). These all results illustrated the great potential of the PVDF/Fe-TA-PEI membrane for efficient oil-water separation.

To evaluate the antifouling properties of the membranes, five cycles of water and emulsion filtration tests were performed on the PVDF, PVDF/Fe-TA and PVDF/Fe-TA-PEI membranes (Fig. 7A). The PVDF membrane showed poor antifouling property with sharp flux decline and limited flux recovery. For the PVDF/Fe-TA and PVDF/Fe-TA-PEI membranes, the permeation fluxes for emulsion filtration could maintain at a high level and the water permeability could almost recover after simple washing processes. Fig. 7B illustrates the permeation fluxes and separation efficiency of the PVDF/Fe-TA-PEI membrane for each emulsion filtration cycle. The permeation fluxes could well maintain above 3000 L m^{-2} h^{-1} and the corresponding separation efficiencies were all above 99.3%. As summarized in Fig. 7C, the water flux of the PVDF/Fe-TA-PEI membrane could recover more than 86% of the original level after five-cycle filtrations. Obviously, the PVDF/Fe-TA-PEI membrane exhibited superior antifouling property comparing with the PVDF membrane. Also, the long-term anti-oil-fouling property of the PVDF/Fe-TA-PEI membrane was also reported (Fig. S8 in Supporting information). After water rinsing, the surface oil fouling was mostly removed and thus the superhydrophilicity and underwater superoleophobicity of the PVDF/Fe-TA-PEI membrane were recovered (Fig. S9 in Supporting information). All these results demonstrated that the PVDF/Fe-TA-PEI membrane exhibited excellent antifouling ability and durability for oil-water emulsion separation.

The antifouling mechanism of the PVDF/Fe-TA-PEI membrane was illustrated in Fig. 7D. In detail, hydrophilic hierarchical architecture of the PVDF/Fe-TA-PEI membrane attracted water molecules and confined a hydration layer within micro-patterns of rough structures. When oil droplets were forced to membrane surface by filtration, most oil droplets were rejected by size exclusion effect and accumulated on membrane surface. These accumulated oil droplets would be obstructed out of the hydration layer and readily be swept away from membrane surface by near-surface shear water flow. Overall, the anti-oil-fouling performance of PVDF/Fe-TA-PEI membranes was due to the synergistic effect of hydrophilic chemistries, hierarchical architectures and size exclusion.

In summary, we offered a novel catechol chemistry engineered hierarchical assembly strategy to develop hydrophilic hierarchical Fe-TA-PEI composite PVDF membrane featured with superhydrophilic and underwater superoleophobic wettability for oil/water separation. Benefiting from synergistic effect of Fe^{III}-TA coordination assembly with TA-PEI polyplex electrostatic assembly, the as-prepared PVDF/Fe-TA-PEI membrane was successfully decorated with hierarchical architectures and showed excellent superhydrophilicity, underwater superoleophobicity and anti-oil-adhesion capability. The superhydrophilic feature of the membrane greatly promoted membrane permeability. The underwater superoleophobic and anti-oil-adhesion features contributed to the high-performance application of the membrane in various emulsion separation with high permeation flux, high separation efficiency and excellent antifouling performance. The permeation flux of the membrane reached 3397 L m^{-2} h^{-1}, being almost 4 times that of the original PVDF membrane, and the separation

efficiency was all above 99.3%. Excellent antifouling performance with 93% flux recovery and remarkable recyclability could be achieved in cycled oil-in-water emulsion separation. We proposed that the hierarchical assembly of metal-phenolic-polyplex coating could act as a platform for designing and constructing various superwetting materials for oil-water separation.

Declaration of competing interest

The authors declare that they have no known competing financial interests or personal relationships that could have appeared to influence the work reported in this paper.

Acknowledgments

This work was financially supported by National Natural Science Foundation of China (No. 21706230), China Postdoctoral Science Foundation (No. 2019M652141), National Natural Science Foundation of China (Nos. 22075246 and 21776253), Public Welfare Project of the Science and Technology Committee of Zhejiang Province (No. LGF20B060002), Provincial Key R&D Program of Zhejiang Province (No. 2019C03094).

Supplementary materials

Supplementary material associated with this article can be found, in the online version, at doi:10.1016/j.cclet.2021.12.017.

References

[1] J. Zhang, F. Zhang, J. Song, et al., J. Mater. Chem. A 7 (2019) 20075–20102.
[2] Y. Deng, C. Peng, M. Dai, et al., J. Cleaner Prod. 266 (2020) 121624.
[3] S. Huang, R.H.A. Ras, X. Tian, Curr. Opin. Colloid Interface Sci. 36 (2018) 90–109.
[4] S.P. Nunes, P.Z. Culfaz-Emecen, G.Z. Ramon, et al., J. Membr. Sci. 598 (2020) 117761.
[5] N.H. Ismail, W.N.W. Salleh, A.F. Ismail, et al., Sep. Purif. Technol. 233 (2020) 116007.
[6] E. Tummons, Q. Han, H.J. Tanudjaja, et al., Sep. Purif. Technol. 248 (2020) 116919.
[7] Y. Zhu, D. Wang, L. Jiang, et al., NPG Asia Mater. 6 (2014) e101.
[8] R. Zhang, Y. Liu, M. He, et al., Chem. Soc. Rev. 45 (2016) 5888–5924.
[9] S. Zarghami, T. Mohammadi, M. Sadrzadeh, et al., Prog. Polym. Sci. 98 (2019) 101166.
[10] C. Chen, D. Weng, A. Mahmood, et al., ACS Appl. Mater. Interfaces 11 (2019) 11006–11027.
[11] Z. Chu, Y. Feng, S. Seeger, Angew. Chem. Int. Ed. 54 (2015) 2328–2338.
[12] B. Wang, W. Liang, Z. Guo, et al., Chem. Soc. Rev. 44 (2014) 336–361.
[13] Y. Peng, Z. Guo, J. Mater. Chem. A 4 (2016) 15749–15770.
[14] M. Long, Y. Ma, C. Yang, et al., J. Mater. Chem. A 9 (2021) 1395–1417.
[15] H. Yang, K. Liao, H. Huang, et al., J. Mater. Chem. A 2 (2014) 10225–10230.
[16] S. Gao, J. Sun, P. Liu, et al., Adv. Mater. 28 (2016) 5307–5314.
[17] L. Tang, Z. Zeng, G. Wang, et al., ACS Appl. Mater. Interfaces 11 (2019) 18865–18875.
[18] M. Liu, S. Wang, Z. Wei, et al., Adv. Mater. 21 (2009) 665–669.
[19] Z. Xue, S. Wang, L. Lin, et al., Adv. Mater. 23 (2011) 4270–4273.
[20] D. Tian, X. Zhang, Y. Tian, et al., J. Mater. Chem. 22 (2012) 19652–19657.
[21] S. Zhang, F. Lu, L. Tao, et al., ACS Appl. Mater. Interfaces 5 (2013) 11971–11976.
[22] R. Wang, X. Zhao, N. Jia, et al., ACS Appl. Mater. Interfaces 12 (2020) 10000–10008.
[23] Z.M. Zhang, Z.Q. Gan, R.Y. Bao, et al., J. Membr. Sci. 593 (2020) 117420.
[24] J.K. Pi, J. Yang, Z.K. Xu, J. Membr. Sci. 601 (2020) 117915.
[25] Y. Zhao, Y. Zhang, F. Li, et al., J. Membr. Sci. 627 (2021) 119234.
[26] Y. Zhu, F. Zhang, D. Wang, et al., J. Mater. Chem. A 1 (2013) 5758–5765.
[27] Y. Zhu, J. Wang, F. Zhang, et al., Adv. Funct. Mater. 28 (2018) 1804121.
[28] Y. Tong, C. Zuo, W. Ding, et al., J. Membr. Sci. 628 (2021) 119113.
[29] M. Tao, L. Xue, F. Liu, et al., Adv. Mater. 26 (2014) 2943–2948.
[30] P. Gao, Z. Liu, D.D. Sun, et al., J. Mater. Chem. A 2 (2014) 14082–14088.
[31] L. Zhang, Y. He, P. Luo, et al., J. Mater. Chem. A 8 (2020) 4483–4493.
[32] Z. Wang, S. Ji, J. Zhang, et al., J. Membr. Sci. 564 (2018) 317–327.
[33] L. Shen, X. Wang, Z. Zhang, et al., ACS Appl. Mater. Interfaces 13 (2021) 14653–14661.
[34] Z. Wang, S. Ji, F. He, et al., J. Mater. Chem. A 6 (2018) 3391–3396.
[35] P. Raturi, K. Yadav, J.P. Singh, ACS Appl. Mater. Interfaces 9 (2017) 6007–6013.
[36] L. Zhu, H. Li, Y. Yin, et al., Environ. Sci. Nano 7 (2020) 903–911.
[37] Y. Zhao, X. Yang, L. Yan, et al., J. Membr. Sci. 618 (2021) 118525.
[38] J. Dai, L. Wang, Y. Wang, et al., ACS Appl. Mater. Interfaces 12 (2020) 4482–4493.
[39] Z. Zhu, Z. Li, L. Zhong, et al., J. Membr. Sci. 572 (2019) 73–81.
[40] L. Zhang, Y. Lin, L. Cheng, et al., J. Membr. Sci. 582 (2019) 48–58.
[41] Y. Zhu, W. Xie, F. Zhang, et al., ACS Appl. Mater. Interfaces 9 (2017) 9603–9613.
[42] H. Ejima, J.J. Richardson, K. Liang, et al., Science 341 (2013) 154–157.
[43] H. Ejima, J.J. Richardson, F. Caruso, Nano Today 12 (2017) 136–148.
[44] M.A. Rahim, S.L. Kristufek, S. Pan, et al., Angew. Chem. Int. Ed. 57 (2018) 2–26.
[45] H.J. Kim, D.G. Kim, H. Yoon, et al., Adv. Mater. Interfaces 2 (2015) 1500298.
[46] Y.Z. Song, X. Kong, X. Yin, et al., Colloids Surf. A 522 (2017) 585–592.
[47] Q.Z. Zhong, S. Pan, M.A. Rahim, et al., ACS Appl. Mater. Interfaces 10 (2018) 33721–33729.
[48] M. Li, L. Wu, C. Zhang, et al., Appl. Surf. Sci. 483 (2019) 967–978.
[49] J. Wu, Z. Hou, Z. Yu, et al., Sep. Purif. Technol. 258 (2021) 118022.
[50] X. Zhao, R. Wang, Y. Lan, et al., J. Membr. Sci. 630 (2021) 119310.
[51] X. Zhao, N. Jia, L. Cheng, et al., ACS Omega 4 (2019) 2320–2330.
[52] N. Sahiner, S. Sagbas, M. Sahiner, et al., Polym. Degrad. Stab. 133 (2016) 152–161.
[53] Q. Li, D.G. Barrett, P.B. Messersmith, et al., ACS Nano 10 (2016) 1317–1324.
[54] M.A. Rahim, K. Kempe, M. Müllner, et al., Chem. Mater. 27 (2015) 5825–5832.
[55] J. Cui, Z. Zhou, A. Xie, et al., J. Membr. Sci. 573 (2019) 226–233.